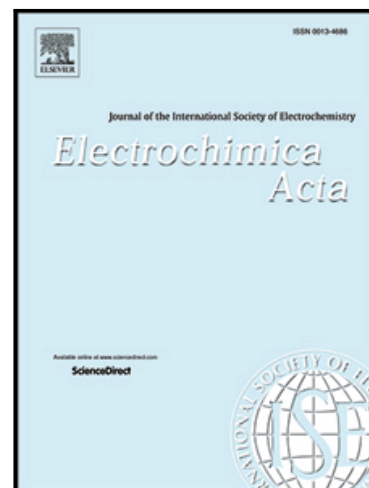


Journal Pre-proof

Enhancement of the electrochemical reduction of CO₂ to methanol and suppression of H₂ evolution over CuO nanowires.

Cátia Azenha , Cecilia Mateos-Pedrero , Manuel Alvarez-Guerra , Angel Irabien , Adélio Mendes

PII: S0013-4686(20)31600-5
DOI: <https://doi.org/10.1016/j.electacta.2020.137207>
Reference: EA 137207



To appear in: *Electrochimica Acta*

Received date: 15 June 2020
Revised date: 15 September 2020
Accepted date: 28 September 2020

Please cite this article as: Cátia Azenha , Cecilia Mateos-Pedrero , Manuel Alvarez-Guerra , Angel Irabien , Adélio Mendes , Enhancement of the electrochemical reduction of CO₂ to methanol and suppression of H₂ evolution over CuO nanowires., *Electrochimica Acta* (2020), doi: <https://doi.org/10.1016/j.electacta.2020.137207>

This is a PDF file of an article that has undergone enhancements after acceptance, such as the addition of a cover page and metadata, and formatting for readability, but it is not yet the definitive version of record. This version will undergo additional copyediting, typesetting and review before it is published in its final form, but we are providing this version to give early visibility of the article. Please note that, during the production process, errors may be discovered which could affect the content, and all legal disclaimers that apply to the journal pertain.

© 2020 Published by Elsevier Ltd.

© 2020. This manuscript version is made available under the CC-BY-NC-ND 4.0 license <http://creativecommons.org/licenses/by-nc-nd/4.0/>

Highlights

- CuO nanowires (NWs) were developed as a highly efficient ER CO_2 electrode
- CuO NWs catalyst outperforms the single metal Cu-catalysts in aqueous environment
- The competing H_2 evolution reaction was significantly suppressed on CuO NWs
- Methanol (faradaic efficiency of 66 %) was selectively produced on CuO NWs
- CuO NWs electrode can be also used in a gas diffusion electrode (GDE) configuration

Journal Pre-proof

Enhancement of the electrochemical reduction of CO₂ to methanol and suppression of H₂ evolution over CuO nanowires.

Cátia Azenha^a, Cecilia Mateos-Pedrero^{a}, Manuel Alvarez-Guerra^b, Angel Irabien^b and
Adélio Mendes^{a*}*

^a LEPABE - Laboratory for Process Engineering, Environment, Biotechnology and Energy,
Faculty of Engineering, University of Porto, Rua Dr. Roberto Frias, 4200-465 Porto,
Portugal.

^b Department of Chemical and Biomolecular Engineering, ETSIIT, University of Cantabria,
Avda. Los Castros, 39005 Santander, Spain

Keywords: CO₂ electroreduction; copper-based catalysts; copper(II) oxide; methanol;
selectivity; GDE-electrodes

Abstract: A highly efficient copper-catalyst (noble-metal free) was developed for the electrochemical reduction of CO₂ (ERCO₂) to methanol. Due to the nanowire structure of the catalyst, a remarkable ERCO₂ selectivity was achieved, while the competing H₂ evolution reaction (HER) was significantly suppressed for the overall range of potential tested. The developed copper-catalyst (CuO NWs) outperforms the single metal Cu-catalysts in aqueous environment. Under atmospheric conditions, methanol was produced at an overpotential of 410 mV with a faradaic efficiency (FE) of 66 %, and 1.27×10^{-4} mol m⁻² s⁻¹ of production yield; which represents a 6.7 % improvement over the previously reported value of 1.19×10^{-4} mol m⁻² s⁻¹. Interestingly, when the developed CuO NWs was used as a gas diffusion electrode (GDE) in a filter-press cell (more *real* industrial configuration), methanol remained as the major ERCO₂ product with the same FE (66 %).

1. Introduction

The increasing global CO₂ concentration, mainly from extensive fossil fuel utilization, is a serious environmental threat that is considered one of the major causes of climate change [1,2]. The electrochemical reduction of CO₂ (ERCO₂) to fuels and chemical feedstock, using renewable electricity represents one promising approach to reduce anthropogenic CO₂ emissions and for the development of a sustainable energy system [3–5]. However, this desired approach imposes major technological challenges before its implementation in large-scale applications [1]. CO₂ is a fully oxidized and thermodynamically stable molecule. Thus, the development of a suitable catalyst, capable of achieving a stable and cost-effective process, with high efficiency and selectivity at low overpotential, is a crucial requirement [2,4].

In aqueous environment, the ERCO₂ reaction competes in selectivity with the hydrogen evolution reaction (HER), particularly at low applied potentials [6]. Therefore, tuning the

ERCO₂ activity and selectivity to the target product while suppressing the HER is critical for improving the energy efficiency of the process [7]. Metal electrodes have been the focus of extensive ERCO₂ research in aqueous solutions at ambient conditions [8]. However, since the earliest studies by Hori *et al.*, it has been identified that most metals preferentially produce H₂ under electrocatalytic conditions, even in the presence of CO₂ [9]. This is because HER has often smaller overpotentials compared to ERCO₂. Consequently, metals that are active for ERCO₂ are also active for HER [10,11]. Systematic studies have been carried out to improve the ERCO₂ selectivity by controlling the electrodes morphology [12–15] and electronic properties (bimetallic alloys) [7,16]. However, up to now, the search for pure metal catalysts that favor ERCO₂ over HER has proved infertile [11]; in fact, effective suppression of the HER has only been reported using precious bimetallic catalysts (AuPd and PbCu) [7,16].

Recent studies have shown that the production of electrodes with nanostructured surfaces is a path for better efficiency and selectivity, in particular for Cu-based catalysts. For instance, Cu₂O rods were used for the production of CO and formic acid with faradaic efficiencies (FE) of *ca.* 40 % and 33 %, respectively [17]. Sen *et al.* reported that copper foams provide high surface roughness, hierarchical porosity, and confinement of reactive species, resulting in the production of formic acid with FE of 37 % at -1.5 V_{Ag/AgCl} [18]. Ethylene and ethanol were identified as ERCO₂ products using polyhedron Cu₂O particles as catalyst, whose FE can be tuned by varying the thickness of the Cu₂O overlayers [19]. It was also reported that multicarbon product formation, mainly ethylene, is favored on copper cubic facets [20]. More recently, Cu nanowires (NWs) were identified as advanced electrocatalysts for CO₂ and CO electroreduction by Raciti *et al.* [3,21] and Ma *et al.* [2]. Especially for the ERCO₂, this type of catalyst requires an overpotential as low as 300 mV to reach a total current density of -1 mA cm⁻², and enables the production of CO with FE of *ca.* 60 % [3].

In the present study, CuO NWs with high surface area were produced using a simple method and non-precious metals. The developed catalyst was initially tested for ER CO_2 using a conventional three-electrode system, showing remarkable activity and selectivity for methanol production under atmospheric conditions and using an ionic liquid-free electrolyte. The catalyst stability under reaction condition was also assessed and improved, resulting in no apparent deactivation after 2 h of electrolysis. Finally, the CuO NWs electrode was evaluated in a continuous ER CO_2 device, working with a gas diffusion electrode (GDE) configuration.

Journal Pre-proof

2. Experimental

Electrode preparation: Electrodes were prepared by anodization of a bare Cu foam, adapted from the work of Wang *et al.* [22]. Cu foam with a thickness of 80 μm (MTI Corp USA) was successively washed with acetone (Sigma-Aldrich, 99.9 %), ultrapure water (18.2 $\text{M}\Omega\text{ cm}^{-1}$ at 25 $^{\circ}\text{C}$, Millipore Milli-Q system), and 3.0 M HCl (Fluka, 37 %) for 30 min under ultrasonic condition to remove organic contaminants and possible oxide layers on the surface. After then, it was rinsed with ultrapure water and dried at 80 $^{\circ}\text{C}$ in a vacuum oven, before using it as the working electrode. A three-electrode setup was used with a carbon rod as counter electrode and an Ag/AgCl/Sat. KCl as reference electrode, connected to an IM6ex electrochemical workstation (Zahner). The electrolyte was 1.0 M KOH (Merck) solution, which was deaerated by bubbling N_2 for at least 30 min before experiments. The Cu foam was electrochemically anodized at room temperature and constant current density of 10 mA cm^{-2} for 10 min to form $\text{Cu}(\text{OH})_2$ NWs. After anodization, samples were rinsed with ultrapure water and annealed at 150 $^{\circ}\text{C}$ for 1.5 h under static air, to dehydration of $\text{Cu}(\text{OH})_2$ to CuO.

Atomic layer deposition of TiO_2 was conducted on a Beneq thin-film system (TFS 200, Beneq Corporation), according to a previous work [23]. TiO_2 was deposited using titanium isopropoxide ($\text{C}_{12}\text{H}_{28}\text{O}_4\text{Ti} \geq 97\%$, Sigma Aldrich) as precursor, and distilled water (H_2O) as oxidizing agent, at 225 $^{\circ}\text{C}$. Ultrahigh purity nitrogen was used as reactant carrier and purge gas, and the reactor was maintained at 400 Pa.

Physicochemical characterization: The morphology and element distribution was obtained by scanning electron microscopy with energy dispersive spectroscopy (SEM-EDS, Phenom XL Desktop SEM). The crystal structure was studied using X-ray diffraction (XRD, PANalytical X'Pert Pro) operating at Bragg-Bretano focusing geometry and using $\text{Cu K}\alpha$

radiation at wavelengths Cu K α 1 = 1.5406 Å and Cu K α 2 = 1.54443 Å. The data was collected at 2 θ angles (20-100°), with a step size of 0.017°. The Debye-Scherrer equation was applied to determine the average crystallite size. X-ray photoelectron spectroscopy (XPS, Kratos AXIS Ultra HAS) was used to identify the chemical composition and valence state. The analysis was carried out with a monochromatic Al K α X-ray source (1486.7 eV), operating at 15 kV (90 W), in FAT mode (Fixed Analyzer Transmission), with a pass energy of 40 eV for regions and 80 eV for survey. Data acquisition was performed with a pressure lower than 1.0×10^{-6} Pa using a charge neutralization system. Binding energies (BE) were calibrated based on the C 1s line at 285 eV from adventitious carbon. The modeling of the spectra was performed using Shirley type background subtraction and peak fitting with Gaussian-Lorentzian peak shape modified by a tail function for asymmetric peaks, following literature recommendations [24–26]. Details on the curve fitting are provided in Table S2. The CO₂ adsorption was studied by CO₂-temperature programmed desorption combined with mass spectrometric analysis (CO₂-TPD-MS, ChemBET Pulsar TPR/TPD). Initially, 10 % CO₂/He flow was continuously pulsed for 1 h at 50 °C; afterward, the CO₂ desorption was monitored by a quadrupole MS (Pfeiffer Vacuum OmniStar GSD 320) in the temperature range of 50 – 700 °C.

Electrochemical measurements: All potentials were referenced to the Ag/AgCl electrode, and the electrochemical measurements were performed at room temperature and atmospheric pressure, in a conventional three-electrode system. Ag/AgCl/Sat. KCl and carbon rod were used as reference and counter electrodes, respectively. The electrolyte was 150 mL of an aqueous solution of 0.1 M KHCO₃ (Alfa Aesar, 99.95% trace metals basis), prepared with 18.2 M Ω cm⁻¹ (at 25 °C) ultrapure water (Millipore Milli-Q system). Linear sweep voltammetry (LSV), with a scan rate of 20 mV s⁻¹, was carried out using an IM6ex

electrochemical workstation (Zahner) in N₂- or CO₂-saturated electrolyte (the electrolyte was bubbled with N₂ or CO₂ for 30 min before the measurement and a blanketing atmosphere was kept during the reads). The potential was swept from 0.0 to -1.8 V, and the current density was measured and recorded. Electrochemical impedance spectroscopy (EIS) measurements were performed in CO₂-saturated 0.1 M KHCO₂, at -1.4 V and -1.8 V with an amplitude of 50 mV and frequency from 1 Mhz to 10 mHz. The data obtained were fitted using the ZView software (Version 3.5, Scribner Associates, USA). Adsorption affinity of OH⁻ as surrogate of CO₂⁻ was examined by oxidative LSV at 20 mV s⁻¹ in N₂-saturated 0.1 M NaOH. The electrodes double-layer capacitance was determined in N₂-saturated 0.1 M KHCO₃ for assessing the surface roughness factor [2]. The cyclic voltammograms (CV) were acquired in the non-faradaic region of the voltammogram at multiple scan rates (5 - 100 mV s⁻¹). The slope of the current density vs scan rate provided the capacitance value, which was normalized to the polycrystalline Cu foil to obtain the surface roughness factor (Figure S6 and Table S3).

CO₂ reduction electrolysis and product analysis: Electrolysis experiments were conducted at atmospheric conditions using the three-electrode cell previously described, and 0.1 M KHCO₃ saturated with CO₂ as electrolyte. For each potential studied, the experiments lasted 120 min and were performed using fresh electrodes and electrolytes.

Gas products generated during CO₂ electrochemical reduction were analyzed using gas chromatography (GC, GC-2010 Plus, Shimadzu), using He as the carrier gas. The GC was equipped with an HP-PLOT Q column (Agilent) and a barrier ionization discharge (BID) detector. GC runs were initiated 20 min after the start of the electrolysis and thereafter every 20 min. To ensure that the reported data is from a system under equilibrium condition, only the average of the third to the sixth GC measurements was used in the data analysis. Liquid

products were collected at the end of the electrolysis and analyzed by headspace GC (Nexis GC-2030, Shimadzu) equipped with a TRB-624 column (Teknokroma), using He as the carrier gas. All measurements were recorded in duplicate to ensure reproducibility. The FE, product formation rate, overpotential, and cell energy efficiency were determined according to the equations presented in supporting information.

Filter press tests: Selected electrodes were tested on a filter-press cell at ambient conditions of pressure and temperature, using an experimental setup described in previous works [27,28]. A Nafion 117 cation exchange membrane was used to separate the cathode and anode compartments, and the geometric electrode area was 10 cm^2 . A tinned steel mesh was used as current collector and a dimensionally stable anode [DSA/O₂ (Ir-MMO (mixed metal oxide) on platinum)] as counter electrode. A leak-free Ag/AgCl 3.4 mol L^{-1} KCl reference electrode was assembled close to the surface of the cathode. An aqueous solution of 0.1 M KHCO_3 (PanReac, > 99 % purity) and 1.0 M KOH (PanReac, 85 % purity) was used as catholyte and anolyte, respectively. Experiments were conducted at galvanostatic conditions (45 mA cm^{-2}), with the current supplied by the potentiostat (MSTAT 4, Arbin Instruments). Each test had the duration of 90 min and was performed on a continuous mode with a single pass of the catholyte and anolyte through the cell with a flow rate of $0.57 \text{ mL min}^{-1} \text{ cm}^{-2}$, using two peristaltic pumps (Watson Marlow 320, Watson Marlow Pumps Group). Pure gaseous CO₂ was fed to the cell at a flow rate of 200 mL min^{-1} . To ensure the reproducibility of the results, each test was conducted in duplicate on different days.

Gas products were analyzed online every 30 min with a micro gas chromatograph (490 Micro GC, Agilent) equipped with four channels (columns: PBQ + MS5A, PoraPLOT U, CP-Sil 5 CB, and CP-WAX 52 CB). Liquid samples were also collected every 30 min and analyzed by ion chromatography to obtain the formate concentration; the analysis was carried out with a

Dionex ICS 1100 equipped with an AS9-HC column, using a solution of 4.5 mmol L⁻¹ of Na₂CO₃ as the eluent at a flow rate of 1 mL min⁻¹. The methanol and ethanol production was accessed by headspace GC (GCMS-QP 2010 Ultra, Shimadzu) equipped with a DB-624 column (Agilent), using He as the carrier gas.

Journal Pre-proof

3. Results and discussion

3.1 Electrodes characterization

A Cu foam was used as substrate for the production of CuO NWs electrodes for the ER CO_2 , using a method adapted from the work of Wang *et al.* [22] (details provided in supporting information). The morphology of the various samples collected at different stages of the electrode preparation was characterized by SEM, as illustrated in Figure 1. As the substrate, the bare pristine foam presents a smooth surface and a 3D interconnected network with a pore size of 100-300 μm (Figure 1a). However, after anodization, the 3-D skeleton of the Cu foam is evenly covered by $\text{Cu}(\text{OH})_2$ NWs with 4-5 nm in length and 0.3-0.6 nm in width (Figures 1b and c). The nanowire morphology and size are maintained after annealing, as depicted in Figure 1d.

The crystal structure of the prepared samples was investigated by XRD. All samples exhibit strong peaks at 43.3° , 50.4° , and 74.1° ascribed to Cu^0 (Figure 1h), which correspond to the bulk structure of the Cu foam substrate. Since the anodization is a surface phenomenon, it was not expected changes in the bulk structure of the samples after treatment. However, and in agreement with the trend reported by Wang *et al.* [22], the main diffraction peaks of $\text{Cu}(\text{OH})_2$ (35 nm, Debye-Scherrer) are detected after anodization. After thermal annealing, broad diffraction peaks at 35.8° (11-1) and 38.7° (111) evidences the appearance of CuO, which confirms the dehydration of most $\text{Cu}(\text{OH})_2$ phase. Compared to $\text{Cu}(\text{OH})_2$ NWs, the broader peaks observed for CuO NWs indicate a decrease in crystallite size (21 nm, Debye-Scherrer). A very weak reflection at 23.9° suggests that some $\text{Cu}(\text{OH})_2$ is still present in the annealed sample.

The surface of the various samples was studied by XPS. For the bare Cu foam, the peak-fit of the Cu $2p_{3/2}$ core level gives a single narrow peak centered at 932.9 eV (Figure 1e, Table S1) that can be attributed to Cu^0 and/or Cu^+ . Thus, the chemical speciation of copper was based

on the Cu LMM Auger peak [26]. The Auger peak-shape in Figure S3a suggests that copper is present, at least, in two different oxidation states characterized by the main peak at 915.9 eV (Cu^+ , 69 at. %) and the shoulder at 918.2 eV (Cu^0 , 31 at. %). After anodization (Figure 1f, Table S1), the Cu $2p_{3/2}$ peak shifted to higher BEs (934.4 eV), and strong shake-up satellite peaks are observed, endorsing the formation of $\text{Cu}(\text{OH})_2$. For the annealed sample (Figure 1g), the values of the Cu $2p_{3/2}$ BE (933.6 eV, Table S1) and Cu LMM (917.4 eV, Table S1) peaks are consistent with the presence of CuO [26].

3.2 Electrochemical performance and stability

The electrocatalytic activity of the prepared electrodes was initially accessed by LSV in N_2 or CO_2 -saturated electrolyte, using a standard three-electrode cell, Figure 2. The LSV curve of the Cu foam recorded in N_2 environment exhibits a clear reduction peak between -0.3 V and -0.7 V, which can be attributed to the reduction of Cu^+ to Cu^0 [29]. XRD and XPS already evidenced the presence of Cu_2O . For $\text{Cu}(\text{OH})_2$ NWs and CuO NWs, two cathodic signals (C_I and C_{II} , Figure S5) are observed, which were assigned to the sequential reduction of Cu^{2+} to Cu^+ and Cu^+ to Cu^0 [29,30].

Under CO_2 -media, the Cu foam exhibits a total current density (j_{tot}) of -12.5 mA cm^{-2} at -1.8 V. However, no major differences are observed in comparison with the LSV response under N_2 -saturated electrolyte, suggesting that the water electrolysis is the dominant reaction (Figure 2a). At the same applied potential range, both $\text{Cu}(\text{OH})_2$ NWs and CuO NWs produce much higher current densities than the bare Cu foam. For instance, a current of -25.0 mA cm^{-2} was recorded at -1.8 V for $\text{Cu}(\text{OH})_2$ NWs, which represents an increase by 2-fold. For CuO NWs, a notable j_{tot} of -56.8 mA cm^{-2} was registered at the same applied potential (improvement by 4-fold). The increase in surface area after the formation of the nanowires

can explain the current density enhancement observed for Cu(OH)₂ NWs and CuO NWs. As shown in Table S3, Cu(OH)₂ NWs and CuO NWs presents a capacitance of 10.3 mF cm⁻² and 9.82 mF cm⁻², respectively. This indicates that the roughness factors are 11 times higher than that of Cu foam (capacitance of 0.93 mF cm⁻²). On the other hand, Cu(OH)₂ NWs and CuO NWs have similar roughness factors, suggesting that the higher current density measured for CuO NWs is indicative of higher activity.

In addition to the high activity, this preliminary test suggests that CuO NWs is highly selective for the ERCO₂. For the overall range of potential tested, the total current density recorded under N₂-environment is almost negligible (*ca.* -1 mA cm⁻²), evidencing that the HER competing reaction was strongly suppressed (Figure 2c). In contrast, after the incorporation of CO₂, the current density sharply increased, indicating high activity/selectivity for the CO₂ reduction. Additionally, the onset potential shifted positively from -1.05 V (Cu foam) to -0.57 V (CuO NWs), which denotes that the electrocatalytic activity is enhanced for the CuO NWs electrode and less energy is needed to initiate the CO₂ reduction. It is also worth mentioning that most of the surface CuO is reduced to Cu⁰ during the ERCO₂, being Cu⁰ the active state of copper (CuO NWs vs CuO NWs after ERCO₂, Table S1).

The stability of the developed CuO NWs electrode was evaluated by short-term electrolysis at an applied potential of -1.8 V, Figure 3a. As observed, during 2 h of operation the j_{tot} declines from -56.8 mA cm⁻² to -18.2 mA cm⁻², indicating that the CuO NWs electrode will not be stable under long-term electrolysis. According to SEM results (Figure 3b and c), the decrease in activity can be related to some damage of the NWs structure during reaction. To improve the stability of the electrode, a TiO₂ layer with *ca.* 5 nm of thickness was deposited by ALD. This technique has already been identified as a viable tool to add ultrathin corrosion protective layers (TiO₂, Al₂O₃, ZnO, HfO, and ZrO₂) to copper surfaces [31,32]. In the

present work, ALD TiO₂ was successfully used to improve the stability of an ERCO₂ catalyst; after the TiO₂ incorporation, the j_{tot} is stable at -32.0 mA cm⁻² during the 2 h test (Figure 3a). Literature reports that Cu NWs are stable under ERCO₂ conditions over 1 h without further treatment [2]. However, in the cited work, the electrolysis was carried out at lower potentials than those used in this study (*ca.* -1 V_{Ag/AgCl}). Thus, the results here presented may be related to the more reductive environment to which the CuO NWs electrode was exposed, which damages the structure of the NWs. The addition of the TiO₂ layer increases the structural robustness, resulting in high catalytic stability and enables the operation at more cathodic potentials. Moreover, the TiO₂ has a negligible impact on the electrode conductivity and ERCO₂ product distribution, Figure S9. On the other hand, it is also observed that the addition of the TiO₂ layer reduces the total current density (-56.8 mA cm⁻² without TiO₂ and -32.0 mA cm⁻² with TiO₂). This behavior can be explained by the blocking of some CuO active centers, according to SEM-EDS and CO₂-TPD-MS results (supporting information). From here, all results reported concern electrodes with TiO₂ protective layer.

3.3 Electrochemical CO₂ reduction

The activity of the prepared electrodes towards the CO₂ reduction was assessed by potentiostatic measurements for 120 min at selected potentials from -1.2 to -1.8 V, using the conventional three-electrode system and CO₂-saturated 0.1 M KHCO₃ as electrolyte.

The geometric current density remained stable throughout the electrolysis, regardless of the electrode and applied potential (Figure S10). GC analysis revealed that H₂ and CO were the only gas products. Similarly, methanol and ethanol were identified as the main liquid products, with propanol also detected for some samples but with a negligible faradaic efficiency (FE < 2 %).

The current density and FE recorded during the constant-potential electrolysis of CO₂ over the different electrodes are displayed in Figure 4. As expected, the bare copper foam presents quite high values of FE for H₂ production, reaching *ca.* 80 % for each potential tested (Figure 4b). This result is in agreement with the work of Min *et al.*, which reports *ca.* 85 % of H₂ FE for a commercial Cu foam tested under similar conditions at -1.0 V_{Ag/AgCl} [33], confirming that this electrode is not suitable for ERCO₂ due to its low selectivity, as suggested by the LSV. Other studies reported in the literature show Cu foams with lower H₂ FE, for instance, 60 % [18] and 16 % [13] at -1.3 V_{Ag/AgCl}. However, these values were obtained with electrodeposited Cu foams and not with commercial materials.

After anodization, the H₂ FE decreased for an average value of 45 %, which represents a reduction by 1.7-fold when compared to the Cu foam (Figure 4b). CO also started to be produced with a maximum FE of 40.4 % at -1.6 V. At this potential, a remarkable value of $2.43 \times 10^{-5} \text{ mol m}^{-2} \text{ s}^{-1}$ was reached for CO production; 30 % higher than the value recently reported by Luo *et al.* for a porous Zn catalyst ($1.86 \times 10^{-5} \text{ mol m}^{-2} \text{ s}^{-1}$) [34]. Methanol and ethanol were also detected, however, with low FE (*ca.* 10 % and 5 % for methanol and ethanol, respectively).

The unique nanostructure of the nanowires produced during the anodization proved to be effective in decreasing the HER activity. However, the H₂ electrolysis can be further inhibited by the dehydration of Cu(OH)₂ to CuO, as depicted in Figure 4d. After annealing, the H₂ FE remained below 15 % in the potential range of -1.6 to -1.2 V, evidencing that CuO NWs is 5.3-times less HER selective when compared to the Cu foam. Withal, alcohols become the main ERCO₂ products. Ethanol was produced with a maximum FE value of 23.5 % recorded at -1.8 V, and the methanol FE exceeded 50 % in the tested potential range. Particularly at -1.4 V, methanol was selectively produced with FE of 66.4 % and a production yield of $1.27 \times 10^{-4} \text{ mol m}^{-2} \text{ s}^{-1}$; a value slightly higher than the literature reference

($1.19 \times 10^{-4} \text{ mol m}^{-2} \text{ s}^{-1}$) [35]. At the same applied potential (-1.4 V), the overpotential for the ER CO_2 to methanol was found to be 410 mV (supplementary information). The energy efficiency for methanol production was also assessed; 31.2 % at -1.4 V, with a maximum of 32.7 % achieved at -1.2 V.

Concerning the methanol production, the values obtained with the CuO NWs electrode are very close to those reported by Yang *et al.* over CuSe electrodes (FE of 77.6 %, j_{tot} of -41.5 mA cm^{-2} and overpotential of 285 mV) [36]. Moreover, since the j_{tot} decreased after the incorporation of the TiO_2 protective layer, it is expected that further improvement of the protection layer results in the performance enhancement of the developed electrode.

The ideal catalyst for the ER CO_2 should also be effective in inhibiting the HER, and much work has been devoted to this subject [7,12–16]. However, hitherto an effective suppression of the HER has only been achieved using precious metals-containing catalysts [7,16]. Recently, Kim *et al.* reported an unprecedented suppression of the HER for a bimetallic catalyst consisting of Pd adatom decoration of active Cu surfaces; a selectivity of 90 % for the CO_2 reduction was achieved at $-1.7 \text{ V}_{\text{Ag}/\text{AgCl}}$ [16]. The other remarkable example is the nearly 100 % selectivity for ER CO_2 achieved using an AuPd bimetallic catalyst, reported by Valenti *et al.* [7]. On the other hand, for pure metals electrodes, the promotion of ER CO_2 over HER has proved infertile [4,11,37]. For instance, it is reported that the FE for HER is *ca.* 30 % on Cu surfaces at $-1.5 \text{ V}_{\text{Ag}/\text{AgCl}}$ [37], and 50 % on CuO at $-1.7 \text{ V}_{\text{Ag}/\text{AgCl}}$ [4]. In contrast, the developed CuO NWs electrode presents an FE for H_2 evolution of only 14.1 % at -1.4 V. Thus, regarding the inhibition of the H_2 production, the developed electrode has a performance comparable to the state-of-the-art precious metal electrodes and outperforms the single Cu-catalysts in aqueous environment. Withal, the CuO NWs electrode has the advantage of being highly selective for ER CO_2 to methanol.

3.4 Understanding the superior performance of CuO NWs

To disclose the crucial factors affecting the electrocatalytic process, and the superior performance of CuO NWs, further electrocatalytic characterization was performed.

The results from the Tafel analysis are given in Figure 5a. The Tafel slope measured for the Cu foam of 136 mV dec^{-1} agrees with previous reports ($130 \pm 7 \text{ mV dec}^{-1}$) [38], and is indicative of a rate-determining initial electron transfer to CO_2 to form an adsorbed $\text{CO}_2^{\bullet-}$ intermediate [8,38]. The overpotential required for this step is typically large due to the poor stabilization of $\text{CO}_2^{\bullet-}$ by the metal surface [8]. In contrast, electrokinetics data for Cu(OH)_2 NWs and CuO NWs support a mechanism that implies a faster first-electron transfer step prior to a chemical rate-determining step (theoretical value of 59 mV dec^{-1}) [1,39]. Mechanistic divergence from rate-determining $1e^-$ transfer suggests that active sites on the surfaces of Cu(OH)_2 NWs and CuO NWs provide better stabilization to $\text{CO}_2^{\bullet-}$. The faster kinetics recorded when Cu(OH)_2 NWs and CuO NWs are used as electrodes can be explained in part by the field-induced reagent concentration theory (FIRC) [40]. According to FIRC, the slow kinetics, due to the low CO_2 concentration close to the catalytic active sites, can be improved by nanostructured electrodes. As reported, the presence of K^+ can stabilize the adsorption of reaction intermediates (*e.g.*, $\text{CO}_2^{\bullet-}$) [41], and the high local electric fields created by high-curvature structures (*e.g.*, tip of nanowires) tend to concentrate electrolyte cations near CO_2 reduction sites. It seems logical to assume that the particular morphology of the CuO and Cu(OH)_2 NWs supported on a 3D substrate could allow a better stabilization of $\text{CO}_2^{\bullet-}$, explaining the observed faster kinetics.

To confirm the change in the binding affinity of $\text{CO}_2^{\bullet-}$, adsorption of OH^- as a surrogate for $\text{CO}_2^{\bullet-}$ was studied. The current response was measured following single oxidative LSV scans,

starting at -1.15 V to -0.25 V, and results are plotted in Figure 5b. As shown, surface OH⁻ adsorption on CuO NWs and Cu(OH)₂ NWs occurs at a potential *ca.* 50 mV lower than that observed for Cu foam. The negative potential shift indicates higher binding energy between reaction sites and intermediates and, thus, stronger stabilization of CO₂^{*-} on the surface of the CuO NWs and Cu(OH)₂ NWs [42,43], following the mechanism proposed by the Tafel analysis.

EIS measurements were performed to further investigate the effect of the catalyst structure on the kinetics of the CO₂ reduction, Figures 5c and 5d. EIS tests were carried out at -1.4 V and -1.8 V. Literature suggests that at low overpotential the reaction kinetics is controlled by charge transfer process, whereas at larger overpotentials becomes dominated by mass diffusion [42]. The obtained Nyquist plots were fitted by the equivalent circuit model [44] (Figure S11), and the corresponding fitted results are summarized in Tables S7 and S8. According to the EIS fitting, all electrodes had similar electrolyte resistance (R_s), with an average value of 22.5 $\Omega \text{ cm}^{-2}$ due to the same electrolyte condition and reactor. At the same time, obvious differences were observed for the charge transfer resistance (R_{ct}) and diffusion resistance (R_d). Results obtained at -1.4 V (Figure 5c) shows that the R_{ct} decreased by 2.5-fold after anodization, suggesting that the presence of the nanowires enhances the electronic interaction at the reaction interfaces during electrolysis. As result of the FIRC effect, the adsorption energy barrier of CO₂ was reduced, facilitating the electron transfer to form CO₂^{*-} [45]. Moreover, the R_d also decreased, being negligible for CuO NWs, indicating that a pore network was created that guides the diffusion of CO₂ to the active centers. The same pattern is observed for the EIS data acquired at -1.8V; however, as expected, the R_d slightly increased (Figure 5d).

As previously mentioned, CO and methanol were selectively produced over Cu(OH)₂ NWs and CuO NWs surfaces, respectively. However, the reaction selectivity of Cu(OH)₂ NWs and

CuO NWs cannot be explained by structural effects. Thus, it is suggested that the chemical environment is the key to the observed differences. As evidenced by XPS, the BE of Cu 2p core level of Cu(OH)₂ NWs is 0.8 eV higher when compared to CuO NWs (Table S1). The higher BE suggests that the electronic density around Cu²⁺ is smaller, possibly due to the electrons in the outer layer of Cu²⁺ being attracted by the O-H bond. The higher electronic density of the CuO NWs indicates higher basicity and, therefore, higher CO₂ and CO adsorption capacity. This evidence suggests that CuO NWs is capable of stabilizing the CO intermediate, resulting in the conversion of CO₂ to high-reduced products, like methanol. In contrast, the lower CO affinity of Cu(OH)₂ NWs, in respect to CuO NWs, leads to its facile desorption, and thus gaseous CO production.

3.5 CO₂ reduction in a gas-phase GDE configuration

It is also important to highlight that the direct synthesis of the CuO NWs on the surface of a copper foam enables the direct application of the developed electrode in a gas-phase GDE configuration. The GDE reactors provide some significant advantages over the liquid-phase systems. They overcome the low solubility of CO₂ in aqueous electrolytes (33 mM) that hinders high productivity, and are suitable for continuous operation and industrial scale-up [46,47]. Thus, as the gas configurations are closer to a *real* industrial technology, Cu foam and CuO NWs were tested in a filter-press cell working at a constant current density of -45 mA cm⁻², according to previous reports [27,28]. All the tests were carried out at atmospheric conditions in a continuous mode, with a single pass of the catholyte and anolyte through the electrochemical cell. Figure 6 and Table S9 presents the obtained FE and product rate formation.

As observed, the H₂ production from the HER reaction accounts for 47.9 % of the total FE for the Cu foam, with a partial current density of -21.6 mA cm⁻². This value is lower when compared to *ca.* 80 % recorded using the three-electrode cell (Figure 4b), suggesting that the HER is less promoted in the GDE configuration. Thus, besides the advantages already discussed, this result highlights that a major benefit of the GDE configuration, over the liquid-phase systems, is the inhibition of the competing HER. For CuO NWs, an H₂ FE < 15 % was achieved, in agreement with the results obtained in the conventional cell, being HCOO⁻ also identified as ERCO₂ product (FE of 14.9 %). Notwithstanding, methanol was the major ERCO₂ product with an FE of 66.1 % (partial current density of -29.7 mA cm⁻²) and a formation rate of 5.14×10^{-5} mol m⁻² s⁻¹. The FE is comparable to the value obtained at -1.4 V in the conventional system; however, the production yield decreased by 2.5-fold, possibly due to the larger area of the electrode (10 cm²). Thus, the achieved methanol yield is lower when compared to the values reported by Le *et al.* using Cu₂O as electrode (*ca.* 1.19×10^{-4} mol m⁻² s⁻¹), but was recorded with a higher FE value (66 % vs 38 % reported by Le *et al.*) [35].

4. Conclusion

The developed CuO NWs catalyst proved to be very efficient for the ER CO_2 . In aqueous environment, a high current density was obtained (-56.8 mA cm^2 at $-1.8 \text{ V}_{\text{Ag}/\text{AgCl}}$), however with some stability issues that were overcome by depositing a thin layer of TiO_2 on the surface of the catalyst. Using the developed catalyst, methanol was selectively produced with an FE of 66.4 % and energy efficiency of 31.2 % at -1.4 V . The overpotential for CO_2 reduction to methanol was 410 mV, and the production yield $1.27 \times 10^{-4} \text{ mol m}^{-2} \text{ s}^{-1}$. These are quite promising values obtained with a single metal catalyst; and, since the current work has been focused on the demonstration of concept and feasibility, the target of future work will be the performance improvement.

The remarkable catalytic activity of CuO NWs is due to the particular nanostructure of the nanowires that lowers the CO_2 adsorption energy barrier, enhancing the electron transfer to form $\text{CO}_2^{\bullet-}$. The stabilization of the $\text{CO}_2^{\bullet-}$ intermediate is also facilitated by CuO NWs, resulting in the conversion of CO_2 to more reduced products (methanol). Moreover, the network of pores created drives the CO_2 to the active sites, decreasing the diffusion resistance.

The performance of the CuO NWs catalyst was also explored in a continuous-GDE reactor configuration. The direct application of this type of material on a GDE configuration was confirmed, and methanol was the main ER CO_2 product with high efficiency (FE of 66.1 % and partial current density of -30 mA cm^{-2}).

Credit Author Statement

The authors declare that the manuscript entitled “*Enhancement of the electrochemical reduction of CO_2 to methanol and suppression of H_2 evolution over CuO nanowires*”, which has been submitted for publication in the *Electrochimica Acta* Journal has been written

through the contributions of all authors. All authors have approved the final version of the manuscript.

Acknowledgments

Azenha, C., is grateful to the Portuguese Foundation for Science and Technology (FCT) for the doctoral grant (reference SFRH/BD/128768/2017). This work was performed under the project “SunStorage - Harvesting and storage of solar energy”, with reference POCI-01-0145-FEDER-016387, funded by European Regional Development Fund (ERDF), through COMPETE 2020 - Operational Programme for Competitiveness and Internationalisation (OPCI), and by national funds, through FCT - Fundação para a Ciência e a Tecnologia I.P. The authors are thankful to POCI-01-0145-FEDER-006939 (Laboratory for Process Engineering, Environment, Biotechnology and Energy – UID/EQU/00511/2013) funded by the European Regional Development Fund (ERDF), through COMPETE2020 - Programa Operacional Competitividade e Internacionalização (POCI) and by national funds, through FCT - Fundação para a Ciência e a Tecnologia and NORTE-01-0145-FEDER-000005 – LEPABE-2-ECO-INNOVATION, supported by North Portugal Regional Operational Programme (NORTE 2020), under the Portugal 2020 Partnership Agreement, through the European Regional Development Fund (ERDF).

Supporting Information

Details of nanowires formation, XPS details, roughness factors, stability of the CuO NWs electrode, LSV and EIS results, and product distribution data.

Corresponding Author

* Email: cmpedrero@fe.up.pt

* Email: mendes@fe.up.pt

Author Contributions

The manuscript was written through the contributions of all authors. All authors have approved the final version of the manuscript.

Journal Pre-proof

References

- [1] Q. Lu, J. Rosen, Y. Zhou, G.S. Hutchings, Y.C. Kimmel, J.G. Chen, F. Jiao, A selective and efficient electrocatalyst for carbon dioxide reduction, *Nat. Commun.* 5 (2014) 3242. doi:10.1038/ncomms4242.
- [2] M. Ma, K. Djanashvili, W.A. Smith, Selective electrochemical reduction of CO₂ to CO on CuO-derived Cu nanowires, *Phys. Chem. Chem. Phys.* 17 (2015) 20861–20867. doi:10.1039/C5CP03559G.
- [3] D. Raciti, K.J. Livi, C. Wang, Highly Dense Cu Nanowires for Low-Overpotential CO₂ Reduction, *Nano Lett.* 15 (2015) 6829–6835. doi:10.1021/acs.nanolett.5b03298.
- [4] D. Ren, J. Fong, B.S. Yeo, The effects of currents and potentials on the selectivities of copper toward carbon dioxide electroreduction, *Nat. Commun.* 9 (2018) 925. doi:10.1038/s41467-018-03286-w.
- [5] M. Schreier, F. Héroguel, L. Steier, S. Ahmad, J.S. Luterbacher, M.T. Mayer, J. Luo, M. Grätzel, Solar conversion of CO₂ to CO using Earth-abundant electrocatalysts prepared by atomic layer modification of CuO, *Nat. Energy.* 2 (2017) 17087. doi:10.1038/nenergy.2017.87.
- [6] M.-J. Cheng, E.L. Clark, H.H. Pham, A.T. Bell, M. Head-Gordon, Quantum Mechanical Screening of Single-Atom Bimetallic Alloys for the Selective Reduction of CO₂ to C₁ Hydrocarbons, *ACS Catal.* 6 (2016) 7769–7777. doi:10.1021/acscatal.6b01393.
- [7] M. Valenti, N.P. Prasad, R. Kas, D. Bohra, M. Ma, V. Balasubramanian, L. Chu, S. Gimenez, J. Bisquert, B. Dam, W.A. Smith, Suppressing H₂ Evolution and Promoting Selective CO₂ Electroreduction to CO at Low Overpotentials by Alloying Au with Pd, *ACS Catal.* 9 (2019) 3527–3536. doi:10.1021/acscatal.8b04604.
- [8] Y. Chen, C.W. Li, M.W. Kanan, Aqueous CO₂ Reduction at Very Low Overpotential

- on Oxide-Derived Au Nanoparticles, *J. Am. Chem. Soc.* 134 (2012) 19969–19972. doi:10.1021/ja309317u.
- [9] Y. Hori, H. Wakebe, T. Tsukamoto, O. Koga, Electrocatalytic process of CO selectivity in electrochemical reduction of CO₂ at metal electrodes in aqueous media, *Electrochim. Acta.* 39 (1994) 1833–1839. doi:10.1016/0013-4686(94)85172-7.
- [10] A.A. Peterson, F. Abild-Pedersen, F. Studt, J. Rossmeisl, J.K. Nørskov, How copper catalyzes the electroreduction of carbon dioxide into hydrocarbon fuels, *Energy Environ. Sci.* 3 (2010) 1311. doi:10.1039/c0ee00071j.
- [11] Z. Zhao, G. Lu, Computational Screening of Near-Surface Alloys for CO₂ Electroreduction, *ACS Catal.* 8 (2018) 3885–3894. doi:10.1021/acscatal.7b03705.
- [12] W. Luo, W. Xie, M. Li, J. Zhang, A. Züttel, 3D hierarchical porous indium catalyst for highly efficient electroreduction of CO₂, *J. Mater. Chem. A.* 7 (2019) 4505–4515. doi:10.1039/C8TA11645H.
- [13] A. Dutta, M. Rahaman, N.C. Luedi, M. Mohos, P. Broekmann, Morphology Matters: Tuning the Product Distribution of CO₂ Electroreduction on Oxide-Derived Cu Foam Catalysts, *ACS Catal.* 6 (2016) 3804–3814. doi:10.1021/acscatal.6b00770.
- [14] W. Tang, A.A. Peterson, A.S. Varela, Z.P. Jovanov, L. Bech, W.J. Durand, S. Dahl, J.K. Nørskov, I. Chorkendorff, The importance of surface morphology in controlling the selectivity of polycrystalline copper for CO₂ electroreduction, *Phys. Chem. Chem. Phys.* 14 (2012) 76–81. doi:10.1039/C1CP22700A.
- [15] L. Cao, D. Raciti, C. Li, K.J.T. Livi, P.F. Rottmann, K.J. Hemker, T. Mueller, C. Wang, Mechanistic Insights for Low-Overpotential Electroreduction of CO₂ to CO on Copper Nanowires, *ACS Catal.* 7 (2017) 8578–8587. doi:10.1021/acscatal.7b03107.
- [16] C. Kim, T. Möller, J. Schmidt, A. Thomas, P. Strasser, Suppression of Competing Reaction Channels by Pb Adatom Decoration of Catalytically Active Cu Surfaces

- During CO₂ Electroreduction, ACS Catal. 9 (2019) 1482–1488. doi:10.1021/acscatal.8b02846.
- [17] C.W. Li, M.W. Kanan, CO₂ Reduction at Low Overpotential on Cu Electrodes Resulting from the Reduction of Thick Cu₂O Films, J. Am. Chem. Soc. 134 (2012) 7231–7234. doi:10.1021/ja3010978.
- [18] S. Sen, D. Liu, G.T.R. Palmore, Electrochemical Reduction of CO₂ at Copper Nanofoams, ACS Catal. 4 (2014) 3091–3095. doi:10.1021/cs500522g.
- [19] D. Ren, Y. Deng, A.D. Handoko, C.S. Chen, S. Malkhandi, B.S. Yeo, Selective Electrochemical Reduction of Carbon Dioxide to Ethylene and Ethanol on Copper(I) Oxide Catalysts, ACS Catal. 5 (2015) 2814–2821. doi:10.1021/cs502128q.
- [20] F.S. Roberts, K.P. Kuhl, A. Nilsson, High Selectivity for Ethylene from Carbon Dioxide Reduction over Copper Nanocube Electrocatalysts, Angew. Chemie Int. Ed. 54 (2015) 5179–5182. doi:10.1002/anie.201412214.
- [21] D. Raciti, L. Cao, K.J.T. Livi, P.F. Rottmann, X. Tang, C. Li, Z. Hicks, K.H. Bowen, K.J. Hemker, T. Mueller, C. Wang, Low-Overpotential Electroreduction of Carbon Monoxide Using Copper Nanowires, ACS Catal. 7 (2017) 4467–4472. doi:10.1021/acscatal.7b01124.
- [22] Z. Wang, Y. Zhang, H. Xiong, C. Qin, W. Zhao, X. Liu, Yucca fern shaped CuO nanowires on Cu foam for remitting capacity fading of Li-ion battery anodes, Sci. Rep. 8 (2018) 6530. doi:10.1038/s41598-018-24963-2.
- [23] J. Maçaira, L. Andrade, A. Mendes, Highly efficient SiO₂/TiO₂ composite photoelectrodes for dye-sensitized solar cells, Sol. Energy. 158 (2017) 905–916. doi:10.1016/j.solener.2017.10.056.
- [24] F. Cocco, B. Elsener, M. Fantauzzi, D. Atzei, A. Rossi, Nanosized surface films on brass alloys by XPS and XAES, RSC Adv. 6 (2016) 31277–31289.

doi:10.1039/C5RA23135C.

- [25] M.C. Biesinger, L.W.M. Lau, A.R. Gerson, R.S.C. Smart, Resolving surface chemical states in XPS analysis of first row transition metals, oxides and hydroxides: Sc, Ti, V, Cu and Zn, *Appl. Surf. Sci.* 257 (2010) 887–898. doi:10.1016/j.apsusc.2010.07.086.
- [26] M.C. Biesinger, Advanced analysis of copper X-ray photoelectron spectra, *Surf. Interface Anal.* 49 (2017) 1325–1334. doi:10.1002/sia.6239.
- [27] G. Díaz-Sainz, M. Alvarez-Guerra, J. Solla-Gullón, L. García-Cruz, V. Montiel, A. Irabien, Catalyst coated membrane electrodes for the gas phase CO₂ electroreduction to formate, *Catal. Today.* (2018). doi:10.1016/j.cattod.2018.11.073.
- [28] G. Díaz-Sainz, M. Alvarez-Guerra, J. Solla-Gullón, L. García-Cruz, V. Montiel, A. Irabien, CO₂ electroreduction to formate: Continuous single-pass operation in a filter-press reactor at high current densities using Bi gas diffusion electrodes, *J. CO₂ Util.* 34 (2019) 12–19. doi:10.1016/j.jcou.2019.05.035.
- [29] S. González, M. Pérez, M. Barrera, A.R. González Elipe, R.M. Souto, Mechanism of Copper Passivation in Aqueous Sodium Carbonate–Bicarbonate Solution Derived from Combined X-ray Photoelectron Spectroscopic and Electrochemical Data, *J. Phys. Chem. B.* 102 (1998) 5483–5489. doi:10.1021/jp981069k.
- [30] A. Eilert, F. Cavalca, F.S. Roberts, J. Osterwalder, C. Liu, M. Favaro, E.J. Crumlin, H. Ogasawara, D. Friebel, L.G.M. Pettersson, A. Nilsson, Subsurface Oxygen in Oxide-Derived Copper Electrocatalysts for Carbon Dioxide Reduction, *J. Phys. Chem. Lett.* 8 (2017) 285–290. doi:10.1021/acs.jpcclett.6b02273.
- [31] J.S. Daubert, G.T. Hill, H.N. Gotsch, A.P. Gremaud, J.S. Ovental, P.S. Williams, C.J. Oldham, G.N. Parsons, Corrosion Protection of Copper Using Al₂O₃, TiO₂, ZnO, HfO₂, and ZrO₂ Atomic Layer Deposition, *ACS Appl. Mater. Interfaces.* 9 (2017) 4192–4201. doi:10.1021/acsami.6b13571.

- [32] A.I. Abdulagatov, Y. Yan, J.R. Cooper, Y. Zhang, Z.M. Gibbs, A.S. Cavanagh, R.G. Yang, Y.C. Lee, S.M. George, Al₂O₃ and TiO₂ Atomic Layer Deposition on Copper for Water Corrosion Resistance, *ACS Appl. Mater. Interfaces*. 3 (2011) 4593–4601. doi:10.1021/am2009579.
- [33] S. Min, X. Yang, A.-Y. Lu, C.-C. Tseng, M.N. Hedhili, L.-J. Li, K.-W. Huang, Low overpotential and high current CO₂ reduction with surface reconstructed Cu foam electrodes, *Nano Energy*. 27 (2016) 121–129. doi:10.1016/j.nanoen.2016.06.043.
- [34] W. Luo, J. Zhang, M. Li, A. Züttel, Boosting CO Production in Electrocatalytic CO₂ Reduction on Highly Porous Zn Catalysts, *ACS Catal.* 9 (2019) 3783–3791. doi:10.1021/acscatal.8b05109.
- [35] M. Le, M. Ren, Z. Zhang, P.T. Sprunger, R.L. Kurtz, J.C. Flake, Electrochemical Reduction of CO₂ to CH₃OH at Copper Oxide Surfaces, *J. Electrochem. Soc.* 158 (2011) E45. doi:10.1149/1.3561636.
- [36] D. Yang, Q. Zhu, C. Chen, H. Liu, Z. Liu, Z. Zhao, X. Zhang, S. Liu, B. Han, Selective electroreduction of carbon dioxide to methanol on copper selenide nanocatalysts, *Nat. Commun.* 10 (2019) 677. doi:10.1038/s41467-019-08653-9.
- [37] K.P. Kuhl, T. Hatsukade, E.R. Cave, D.N. Abram, J. Kibsgaard, T.F. Jaramillo, Electrocatalytic Conversion of Carbon Dioxide to Methane and Methanol on Transition Metal Surfaces, *J. Am. Chem. Soc.* 136 (2014) 14107–14113. doi:10.1021/ja505791r.
- [38] Y. Peng, T. Wu, L. Sun, J.M. V. Nsanzimana, A.C. Fisher, X. Wang, Selective Electrochemical Reduction of CO₂ to Ethylene on Nanopores-Modified Copper Electrodes in Aqueous Solution, *ACS Appl. Mater. Interfaces*. 9 (2017) 32782–32789. doi:10.1021/acсами.7b10421.
- [39] Y. Chen, M.W. Kanan, Tin Oxide Dependence of the CO₂ Reduction Efficiency on

- Tin Electrodes and Enhanced Activity for Tin/Tin Oxide Thin-Film Catalysts, *J. Am. Chem. Soc.* 134 (2012) 1986–1989. doi:10.1021/ja2108799.
- [40] M. Liu, Y. Pang, B. Zhang, P. De Luna, O. Voznyy, J. Xu, X. Zheng, C.T. Dinh, F. Fan, C. Cao, F.P.G. de Arquer, T.S. Safaei, A. Mepham, A. Klinkova, E. Kumacheva, T. Filleter, D. Sinton, S.O. Kelley, E.H. Sargent, Enhanced electrocatalytic CO₂ reduction via field-induced reagent concentration, *Nature*. 537 (2016) 382–386. doi:10.1038/nature19060.
- [41] J. Resasco, L.D. Chen, E. Clark, C. Tsai, C. Hahn, T.F. Jaramillo, K. Chan, A.T. Bell, Promoter Effects of Alkali Metal Cations on the Electrochemical Reduction of Carbon Dioxide, *J. Am. Chem. Soc.* 139 (2017) 11277–11287. doi:10.1021/jacs.7b06765.
- [42] D. Li, J. Wu, T. Liu, J. Liu, Z. Yan, L. Zhen, Y. Feng, Tuning the pore structure of porous tin foam electrodes for enhanced electrochemical reduction of carbon dioxide to formate, *Chem. Eng. J.* 375 (2019) 122024. doi:10.1016/j.cej.2019.122024.
- [43] S. Zhang, P. Kang, T.J. Meyer, Nanostructured Tin Catalysts for Selective Electrochemical Reduction of Carbon Dioxide to Formate, *J. Am. Chem. Soc.* 136 (2014) 1734–1737. doi:10.1021/ja4113885.
- [44] W. Lv, J. Zhou, F. Kong, H. Fang, W. Wang, Porous tin-based film deposited on copper foil for electrochemical reduction of carbon dioxide to formate, *Int. J. Hydrogen Energy*. 41 (2016) 1585–1591. doi:10.1016/j.ijhydene.2015.11.100.
- [45] D. Li, L. Huang, T. Liu, J. Liu, L. Zhen, J. Wu, Y. Feng, Electrochemical reduction of carbon dioxide to formate via nano-prism assembled CuO microspheres, *Chemosphere*. 237 (2019) 124527. doi:10.1016/j.chemosphere.2019.124527.
- [46] B. Endrődi, G. Bencsik, F. Darvas, R. Jones, K. Rajeshwar, C. Janáky, Continuous-flow electroreduction of carbon dioxide, *Prog. Energy Combust. Sci.* 62 (2017) 133–154. doi:10.1016/j.pecs.2017.05.005.

- [47] J. Song, H. Song, B. Kim, J. Oh, Towards Higher Rate Electrochemical CO₂ Conversion: From Liquid-Phase to Gas-Phase Systems, *Catalysts*. 9 (2019) 224. doi:10.3390/catal9030224.

Journal Pre-proof

Figure captions

Figure 1. SEM image of (a) Cu foam, (b, c) low- and high-magnification of Cu(OH)₂ NWs and (d) CuO NWs. Cu 2p_{3/2} XPS spectrum for (e) Cu foam, (f) Cu(OH)₂ NWs and (g) CuO NWs. XRD pattern of the developed electrodes; ● Cu⁰ (JCPDS card no. 04-0836), ✱ CuO (JCPDS card no. 48-1548), ■ Cu₂O (JCPDS card no. 05-0667) and ◆ Cu(OH)₂ (JCPDS card no. 80-0656).

Figure 2. Current-voltage curves at cathodic potentials in N₂ (dashed lines) and CO₂-saturated (full lines) 0.1 M KHCO₃ for (a) Cu foam, (b) Cu(OH)₂ NWs and (c) CuO NWs. Scan rate, 20 mV s⁻¹.

Figure 3. (a) Dependence of the total current density (i_{tot}) on time with and without the TiO₂ protection layer, recorded at -1.8 V. SEM image of the CuO NWs electrode (a) before electrolysis and (b) after 2 h of electrolysis without the TiO₂ layer.

Figure 4. (a) Total current density and faradaic efficiency over (b) Cu foam, (c) Cu(OH)₂ NWs, and (d) CuO NWs, at different applied potentials.

Figure 5. (a) Tafel plots of the CO₂ reduction partial current density. (b) Single oxidative LSV scans at 50 mV s⁻¹ in N₂-saturated 0.1 M NaOH. Nyquist plots, with fitting curves (dashed lines), of the prepared electrodes in CO₂-saturated 0.1 M KHCO₃ with a frequency from 1 MHz to 10 mHz and 50 mV amplitude at (c) -1.4 V and (d) -1.8 V.

Figure 6. (a) Faradaic efficiencies and (b) production yield for Cu foam and CuO NWs, working on a continuous mode with a single pass of the catholyte and anolyte through the electrochemical cell at a current density of -45 mA cm⁻².

Figures

Figure 1

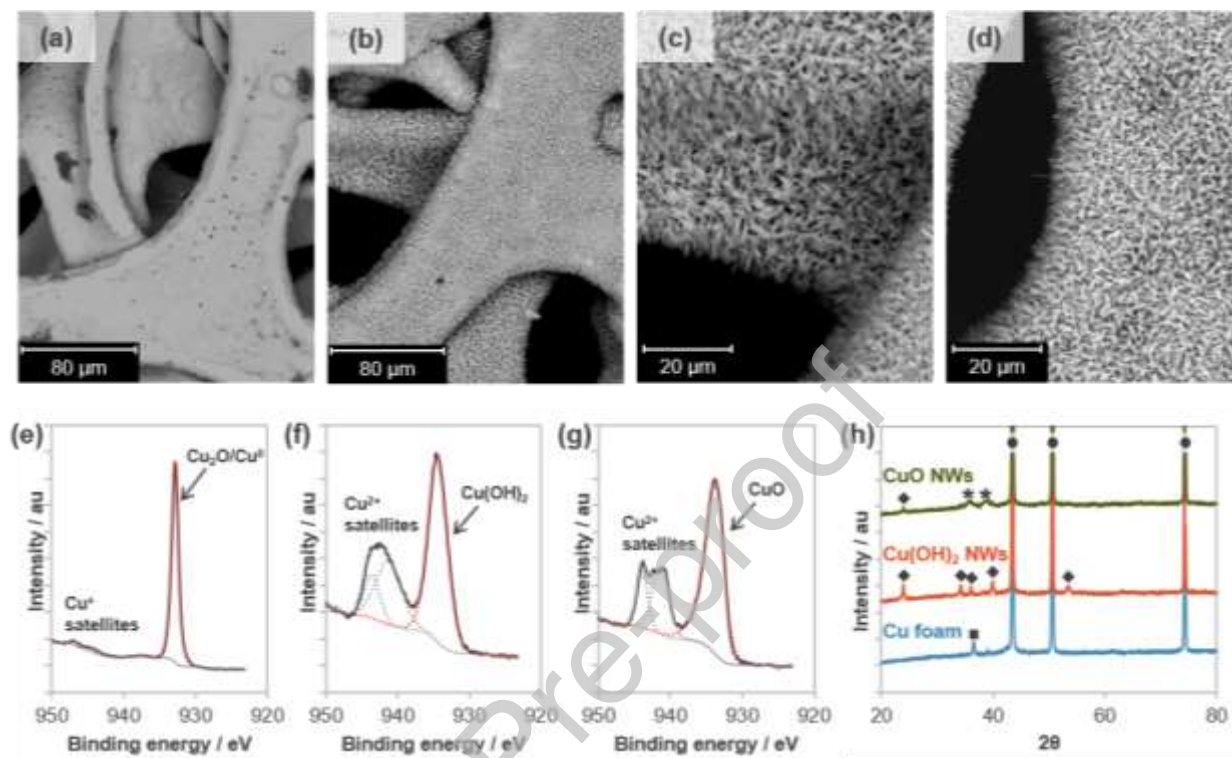
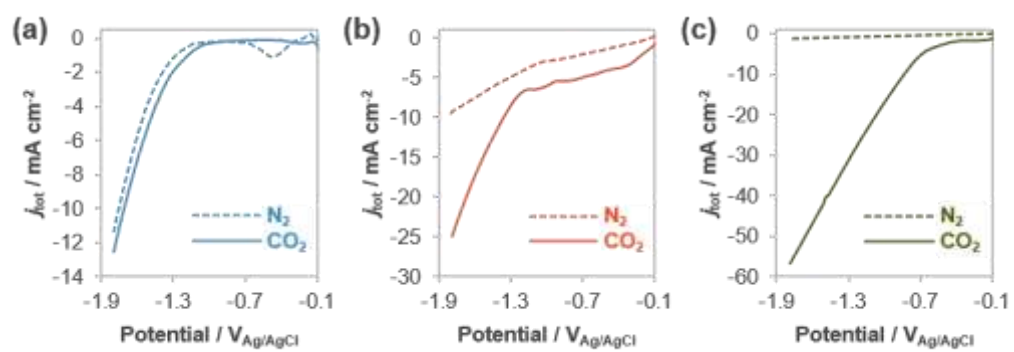


Figure 2



Journal Pre-proof

Figure 3

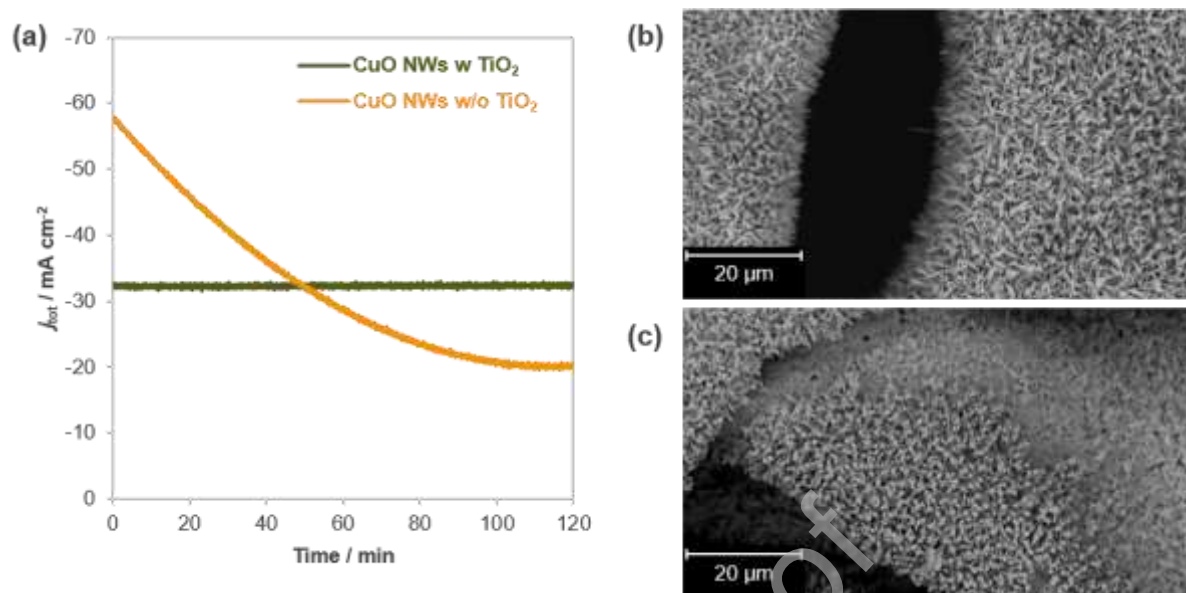


Figure 4

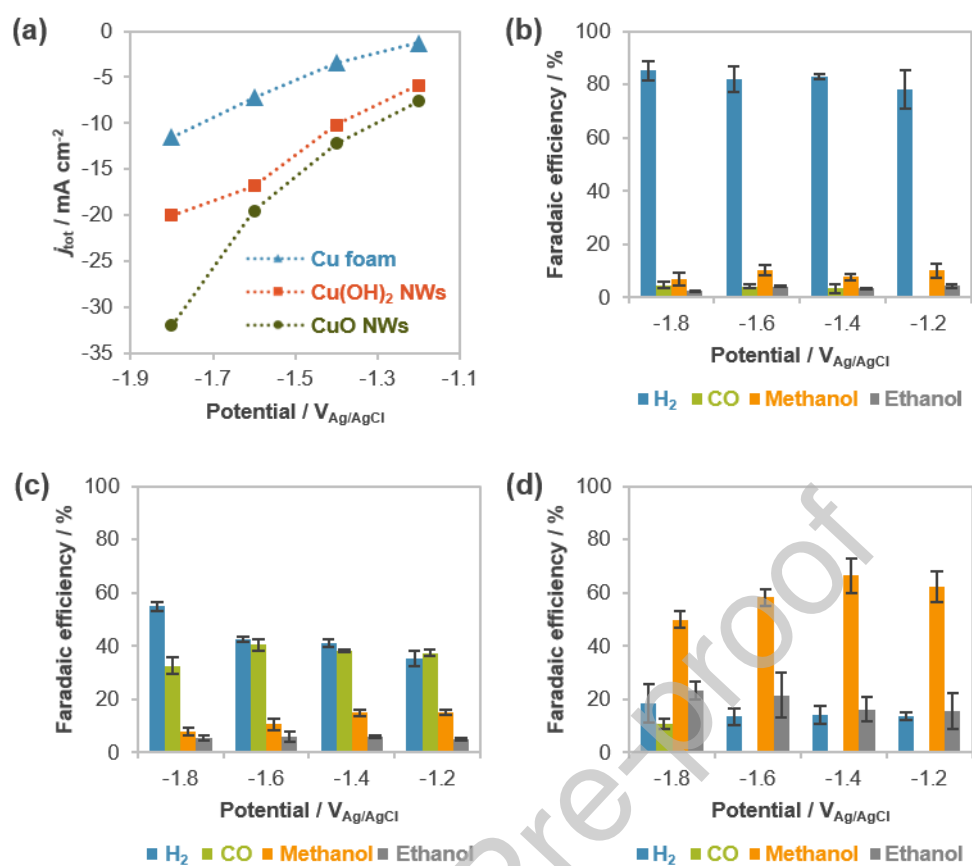


Figure 5

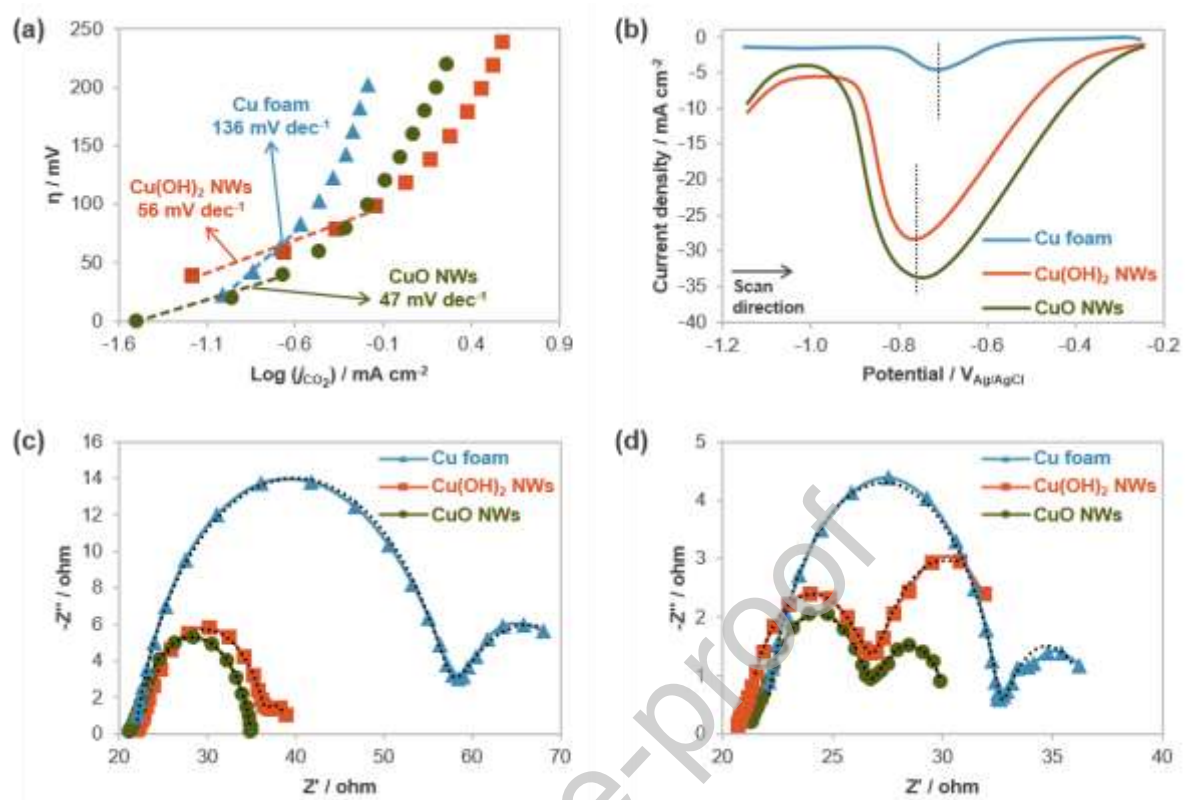
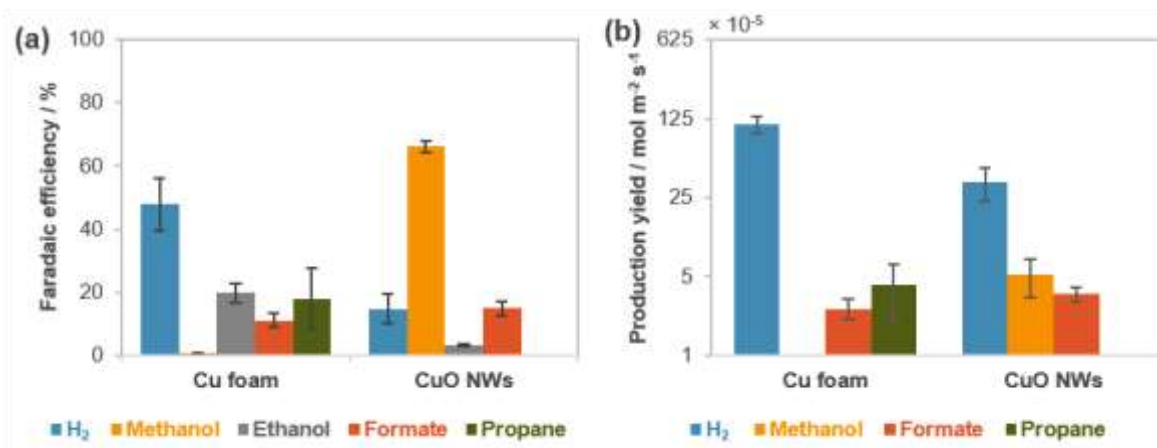


Figure 6



Journal Pre-proof

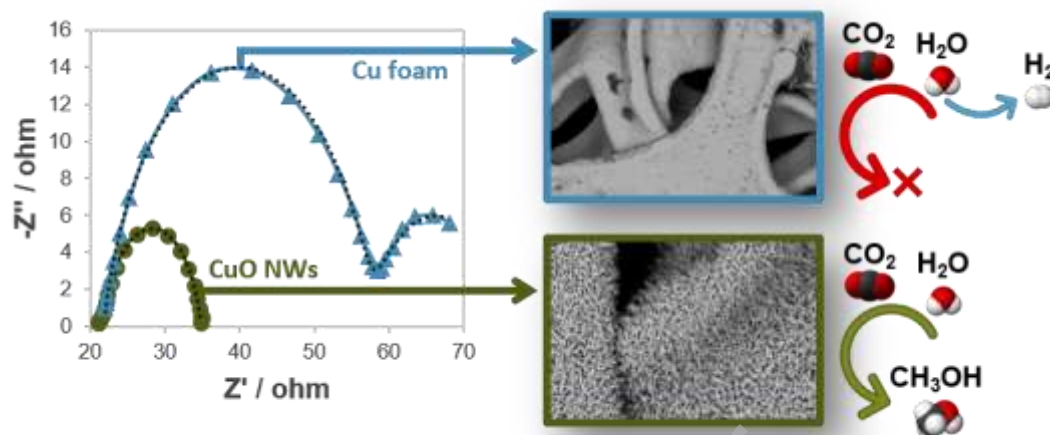
Declaration of interests

The authors declare that they have no known competing financial interests or personal relationships that could have appeared to influence the work reported in this paper.

The authors declare the following financial interests/personal relationships which may be considered as potential competing interests:

Journal Pre-proof

Graphical abstract



Journal Pre-proof